Geohazard Mechanics 1 (2023) 231–243

Contents lists available at ScienceDirect

Geohazard Mechanics

journal homepage: www.keaipublishing.com/en/journals/geohazard-mechanics

Research on the effects of heating and cooling processes on the mechanical properties of yellow rust granite

Luming Zhou [a,b], Zhende Zhu [a,*], Erkan Oterkus [b], Selda Oterkus [b], Huicong Xu [c]

[a] Key Laboratory of Ministry of Education for Geomechanics and Embankment Engineering, Hohai University, Nanjing, 210098, China
[b] Peridynamics Research Center, Department of Naval Architecture, Ocean and Marine Engineering, University of Strathclyde, Glasgow, G4 0LZ, UK
[c] Department of Civil and Environmental Engineering, University of Strathclyde, Glasgow, G1 1XJ, UK

ARTICLE INFO

Keywords:
Granite
Natural cooling
Water cooling cycle
Mechanical characteristics
Damage constitutive model

ABSTRACT

Geological hazards caused by high-temperature rocks cooling down after encountering water are closely related to underground mining and tunneling projects. To fully understand the impact of temperature changes on the mechanical properties of rocks, yellow rust granite samples were subjected to heating-natural cooling and heating-water cooling cycles to experimentally study the effects of these processes on the mechanical properties of the samples. The mechanism of the heating-cooling process on the macromechanical properties of the rock was discussed. Based on the Drucker-Prager criterion and Weibull distribution function, a damage variable correction factor was introduced to reflect the post-peak strain softening characteristics, and a thermo-mechanical coupled damage constitutive model of the granite was established. The results showed that in the natural cooling mode, the mechanical properties deteriorate significantly when the temperature exceeded 600 °C, and the failure mode changed from brittle failure to ductile failure. In the water cooling mode, the peak strength and deformation modulus increased at temperatures below 400 °C with an increase in the cycle number, while at 600 °C, the peak strength and elastic modulus notably decreased. The peak strain increased with the increase of the cycle number and temperature at all temperatures, and the failure mode of the granite tended to change from tensile failure mode to shear failure mode. The experimental results were used to validate the damage constitutive model. The shape parameter r and scale parameter S in the Weibull distribution function of the model were used as indicators to reflect the brittleness degree and peak strength. This study helps to understand the behavior of rocks in high-temperature environments, in order to prevent and mitigate potential geological hazards.

1. Introduction

The rock damage caused by thermal effects holds great significance in geological hazard engineering disciplines, such as high-temperature mining, volcanic geotechnical engineering, and nuclear waste disposal [1–3]. In these fields, rocks endure considerable thermal stresses in high-temperature environments, and the consequential thermal damage can trigger instability and failure of rock masses, ultimately leading to engineering disasters. Hence, comprehending thermal damage, specifically the impact of heating-cooling processes on the mechanical properties of rocks and the associated failure mechanisms, becomes paramount [4–8].

Extensive research has been conducted on the alterations in the mechanical and deformation properties of rock samples following heating-cooling processes [9–13]. For instance, Zhang et al. [3] investigated the deformation properties of granite samples under heating-water cooling conditions, specifically focusing on the evolution of porosity and wave velocity. Yang et al. [4] examined the deformation failure behavior of rocks with pre-existing flaws of varying dip angles after heating and natural cooling. Some scholars employed liquid nitrogen to cool rock samples heated at high temperatures [13–15]. Wu et al. [13] compared the variations in the mechanical properties of rocks under natural cooling and liquid nitrogen cooling, and observed a significant reduction in the strength of granite with liquid nitrogen cooling. The fundamental difference among different cooling modes lies in the varying cooling rates. For example, compared to the natural cooling mode achieved by gradual cooling through the surrounding air or environment, the water cooling mode, due to water's high heat capacity and thermal conductivity, rapidly removes heat from the rock, thereby causing sudden temperature changes. Correspondingly, the greater the temperature

* Corresponding author.
E-mail addresses: 190204030004@hhu.edu.cn (L. Zhou), zzdnj@hhu.edu.cn (Z. Zhu).

https://doi.org/10.1016/j.ghm.2023.09.001
Received 26 July 2023; Received in revised form 31 August 2023; Accepted 10 September 2023
Available online 15 September 2023

change within a short period, the larger the generated thermal stress. Consequently, the thermal damage inflicted upon the interior of the rock becomes more severe. While the studies mentioned above primarily focuses on analyzing the impact of different cooling methods on physical and mechanical properties, they only consider single heating and cooling processes. In certain practical rock engineering scenarios, such as deep underground mining or tunnel construction, rock masses undergo temperature cycling due to factors like groundwater, mechanical excavation, and blasting. As a result, these temperature fluctuations can affect the mechanical properties and stability of the engineered structures. Consequently, several researchers have investigated the effects of heating-cooling cycles on deformation parameters and failure modes [16–20]. For instance, Zhu et al. [21] examined the changes in the strength characteristics of granite after subjecting it to 20 cycles of heating-water cooling, while Weng et al. [22] discussed the cracking characteristics of granites under different numbers of heating-cooling cycles. Nine recent laboratory experiments related to this topic are listed in Table 1. However, despite the comprehensive analysis of the alterations in physical, mechanical, and deformation properties following the heating-cooling process, few studies have derived constitutive stress-strain relationships.

Studying the constitutive relationship of high-temperature rocks is crucial for preventing and mitigating geological hazards caused by them. The rock samples analyzed in the study contained numerous statistically distributed microcracks with lengths ranging from 0.01 mm to 1.0 mm. Under loading conditions, these microcracks initiate, propagate, and accumulate in localized areas, eventually leading to visible macrocracks [24]. Currently, rock damage constitutive models can be broadly categorized into macroscopic damage constitutive models, microscopic damage constitutive models, and statistical damage constitutive models. Among these, statistical damage constitutive models are capable of effectively describing the process of damage evolution within rocks and, can also reflect the mechanical mechanisms of rock damage. As a result, these models have been widely applied in recent years [25–29]. Deng et al. [25] proposed a damage constitutive model utilizing the statistical theory of the maximum entropy distribution, which effectively captures the strain softening characteristics of rocks. However, there is no direct correlation between the statistical characteristics of rocks and the parameters in this constitutive model. Other researchers, such as Zhao et al. [26], Cao et al. [27], and Zhang et al. [28], have proposed statistical damage constitutive models that consider strain hardening and softening, the heterogeneity of microdefects, and the stress drop rate after reaching the peak strength. However, these models do not consider the thermal effects. In a different study, Jiang et al. [30] conducted tests on the peak strength of rocks subjected to a heating-water cooling process and established a statistical damage constitutive (SDC) model based on the Mohr-Coulomb strength criterion. Nonetheless, the damage variables in this model do not adequately capture the thermo-mechanical coupling effect.

Hence, in this study, we investigated the impact of heating temperature, cooling mode, and the number of heating-water cooling cycles on the macromechanical properties of rock samples through uniaxial compression tests. Subsequently, we developed an SDC model for granite using the Drucker-Prager (DP) criterion, considering the thermal and cyclic factors. The validity of the model was verified by comparing it with the experimental results obtained in our study. Finally, the relationship between the parameters in the SDC model and the macroscopic mechanical properties of the rock was investigated, to provide a theoretical foundation for the prevention and mitigation of geological hazards such as collapse and roof caving.

2. Experimental design

2.1. Granite sample

The rock samples use in this experiment were obtained from Jining City, Shandong Province, China, and are commercially known as “yellow rust granite.” Yellow rust granite is characterized by its yellow color and hardness. X-ray diffraction (XRD) analysis revealed that the samples were predominantly composed of quartz, albite, and strontium feldspar, with approximate mineral component percentages of 47.8%, 40.6%, and 11.6%, respectively.

To prepare the specimens, a rock cutting machine, a core drilling machine, and an end face cutting mill were utilized. The specimens were shaped into cylinders with dimensions of 50 mm × 100 mm, maintaining an aspect ratio of 2:1. The processed specimens exhibited uniform particle distribution, a stable structure, and a flatness at both ends of less than 0.01 mm. Additionally, there was no development of microcracks. For each temperature condition, at least of three samples were subjected to uniaxial compression tests. Moreover, samples with intermediate results were selected to emphasize the main focus of the research.

2.2. Experimental procedure

The experimental procedure is illustrated in Fig. 1. Initially, the rock samples were dried using an intelligent constant-temperature drying oven (DHG101-4A), as depicted in Fig. 2a. The drying oven had a maximum temperature of 200 °C with an accuracy of ±0.5 °C. During the drying process, the temperature was set to 105 °C and maintained for 24 hours to ensure thorough drying of the samples.

2.2.1. Heating-natural cooling

To differentiate the effects of various cooling methods and cycle numbers, the experiment employed the following heating temperatures based on previous studies (listed in Table 1): 200, 400, 600, 800, and 1000 °C. The processed granite sample was placed inside a KSL-1100X-S muffle furnace, as shown in Fig. 2b. The samples were heated to the designated temperature at a rate of 3 °C/min and maintained at that temperature for 3 hours to ensure uniform and stable heating. Subsequently, the rock samples were allowed to cool naturally to room temperature (20 °C).

Table 1
Testing parameters employed in previous studies.

References	Origin	Maximum temperature (°C)	Heating rate (°C/min)	Constant temp period (h)	Cooling down ways[a]	Cycle[b]
Jiang et al. [12]	Shenzhen, China	700	2	3	N	No
Yang et al. [4]	Quanzhou, China	900	5	2	N	No
Qin et al. [20]	Beijing, China	1000	3	2	N	No
Zhang et al. [3]	Hubei, China	900	5	4	N, W	No
Zhao et al. [23]	Linyi, Province	800	10	1	N, W	No
Wu et al. [13]	Shandong, China	600	5	10	N, W, L	No
Sha et al. [14]	Suizhou, China	600	5	4	N, W, L	No
Zhu et al. [21]	Zhangzhou, China	650	10	2	W	Yes
Rong et al. [15]	Macheng, China	300	5	4	N, L	Yes

[a] N, W, and L represent natural cooling, water cooling, and liquid N_2 cooling, respectively.
[b] “Yes” means that the heating–cooling cycle process was conducted, and “No” means that the process was conducted only once.

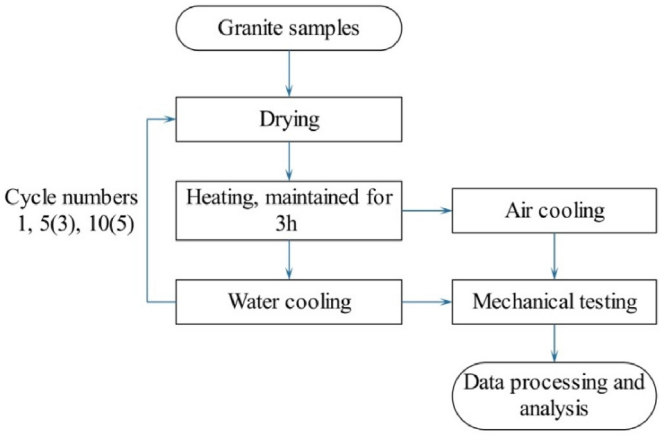

Fig. 1. Flowchart of the experiment.

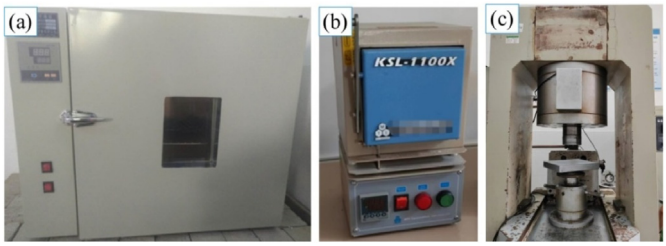

Fig. 2. Experimental instrument: (a) DHG101-4A intelligent constant-temperature drying oven; (b) KSL-1100X-S muffle furnace; and (c) RMT-150B rock mechanics testing machine.

2.2.2. Heating-water cooling cycle

After heating the rock sample to the designated temperature and maintaining it for 2 h, as mentioned earlier, the samples were immersed in a water bath at a constant temperature for an additional 2 h to ensure complete cooling to match the water temperature. Subsequently, the samples were dried once again, representing a single heating-water cooling cycle. The number of cycles at each heating temperature was divided into three categories: 1, 5, and 10 cycles. It is worth noting that during the heating-water cooling cycles with a temperature of 600 °C and five repetitions, a significant number of visible macrocracks developed on the surface of the sample. The sample exhibited extremely low strength and was prone to fracturing. Therefore, the maximum temperature for the heating-water cooling experiment was set at 600 °C, and the number of cycles at this temperature was adjusted to 1, 3, and 5.

2.2.3. Uniaxial compression experiment

The RMT-150B rock mechanics testing machine, as illustrated in Fig. 2c, was used to conduct uniaxial compression tests on the granite specimens under the two cooling modes. The displacement loading method was utilized, with a loading rate of 0.005 mm/s until the rock sample underwent failure. The testing machine automatically generated the stress-strain curve as output.

3. Experimental results

3.1. Heating–natural cooling

3.1.1. Stress–strain curves

The stress-strain curves obtained after the heating-natural cooling process, as shown in Fig. 3, can be divided into four stages. In the first stage, is known as the microcrack compaction stage (OA), the original microcracks within the sample gradually close under the applied compressive stress. This stage is characterized by an upward concave

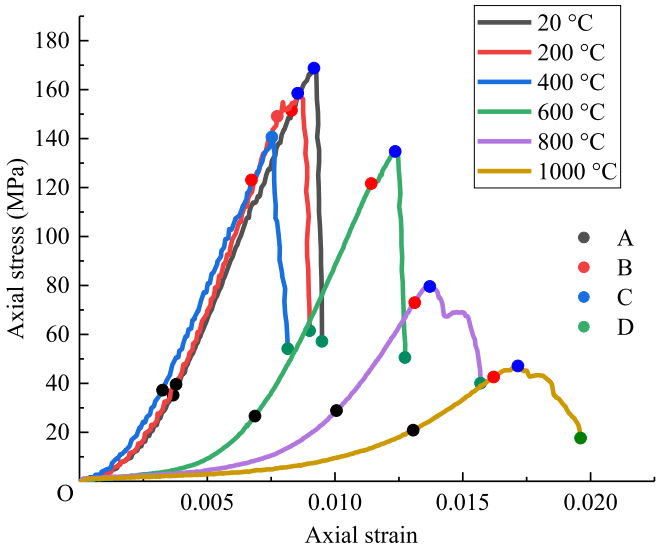

Fig. 3. Stress–strain curves of samples after heating-natural cooling process at different temperatures.

shape of the curve, with the slope gradually increasing as the stress increases. The second stage is the elastic deformation stage (AB), where the stress-strain relationship follows Hooke's law and exhibits linearity. In the third stage, known as the unstable fracture stage (BC), strain softening occurs after reaching point B on the curve. The curve takes a concave shape facing downward, and point C represents the peak strength of the sample. This stage is characterized by the appearance of cracks on the sample surface, often accompanied by audible sounds. Finally, in the fourth stage, known as the destructive stage (CD), the slope of the curve becomes negative, indicating a rapid decrease in stress with increasing strain. The sample undergoes significant deformation and ultimately fails.

As the temperature increases, the microcrack compaction stage (OA) becomes more pronounced, and the peak strength of the rock sample decreases. The elastic modulus remains relatively consistent at temperatures of 20 °C, 200 °C, and 400 °C. However, at temperatures of 600 °C and above, there is a significant decrease in the elastic modulus. This suggests that there is a temperature threshold between 400 °C and 600 °C, beyond which the mechanical properties of the rock deteriorate significantly. Moreover, at temperatures of 800 °C and 1000 °C, the stress-strain curve does not exhibit a sharp decrease after reaching the maximum strength. Instead, there is a noticeable yield step, indicating a transition from brittle to ductile failure mode. The observed phenomena illustrate the following: When the temperature is below 400 °C, water loss occurs within the rock, leading to an increase in porosity, which is the main reason for the slight decrease in specimen strength. On the other hand, when the temperature exceeds 400 °C, mineral boundaries within the rock fracture, resulting in a significant decrease in both strength and deformation capacity. X-ray diffraction results indicate that the granite used in this experiment has a quartz content of 47.8%. The temperature at which quartz undergoes an α-β phase transition is 573 °C. Therefore, when the heating temperature reaches 600 °C or higher, the uneven thermal expansion induced by quartz phase transition and temperature gradients causes thermal stress, which triggers the expansion of grain boundary cracks within the rock and may even lead to transgranular cracks. As a result, the rock's strength rapidly dwindles, and the peak strain significantly increases.

3.1.2. Strength and deformative characteristics

Fig. 4a presents the peak strength and peak strain of granite following the heating-natural cooling process. As the temperature increases from 20 °C to 1000 °C, the peak compressive strength decreases by 6.1%,

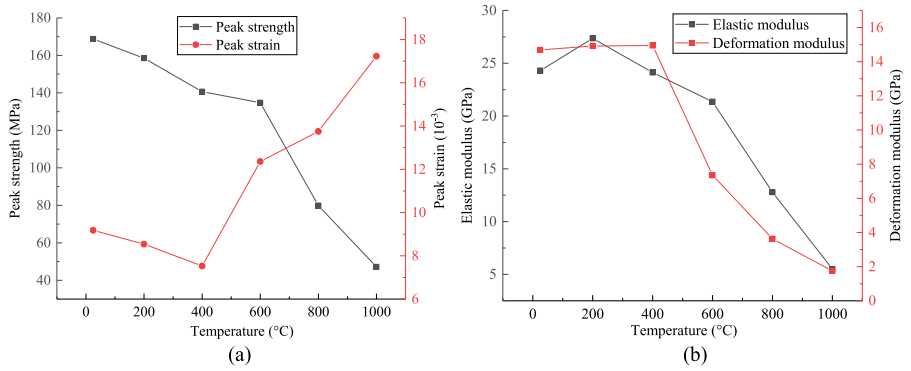

Fig. 4. Mechanical parameters of samples after heating-natural cooling process: (a) Peak strength and peak strain and (b) Elastic modulus and deformation modulus.

11.2%, 4.2%, 40.7%, and 40.9% respectively. This reduction becomes more significant at temperatures of 800 °C and 1000 °C. The decrease in peak strength can be attributed to the evaporation of pore water within the rock, which leads to changes in the crystallization state and internal structure of the sample. Moreover, the elevated heating temperature leading to the thermal stress between mineral particles, resulting in the expansion of microcracks within the rock. Consequently, the rock strength exhibits a monotonic decrease, with the degradation becoming more pronounced at 800 °C.

On the contrary, the peak strain initially decreases by 7.0% and 11.8% at temperatures of 200 °C and 400 °C, respectively. However, it subsequently increases by 64.1%, 11.2%, and 25.3% from 600 °C onwards. The peak strain serves as an effective measure of rock plasticity. The non-monotonic increase in peak strain indicates that temperatures of 200 °C and 400 °C have a minimal impact on the plasticity of the sample. Once the heating temperature exceeds 600 °C, significant damage occurs to the original structure, resulting in the development of additional internal microcracks. Consequently, the plastic characteristics of the rock sample are enhanced.

Fig. 4b displays the elastic modulus and deformation modulus at various temperatures. With, the deformation modulus is used to characterize the stress-strain behavior of a material in the elastic phase. In this experiment, the stress level corresponding to 50% of the compressive strength was chosen for calculating the deformation modulus, which represents the ratio of the stress at the point where the stress is 50% of the peak strength to the corresponding strain. As the heating temperature increases from room temperature to 1000 °C, the elastic modulus initially increases by 12.5% and subsequently decreases by 11.8%, 11.5%, 40.1%, and 56.9%, respectively. Meanwhile, the deformation modulus initially increases by 1.6% and 0.2%, followed by a decrease of 50.8%, 50.7%, and 52%. When considering Figs. 3 and 4 together, the observed trends in the elastic modulus and deformation modulus once again highlight that heating and natural cooling at 200 °C and 400 °C have minimal impact on the strength and deformation characteristics of the rocks. However, at temperatures above 600 °C, there is a significant decrease in strength and a considerable increase in ductility. Moreover, as the temperature continues to rise, the extent of these changes expands further.

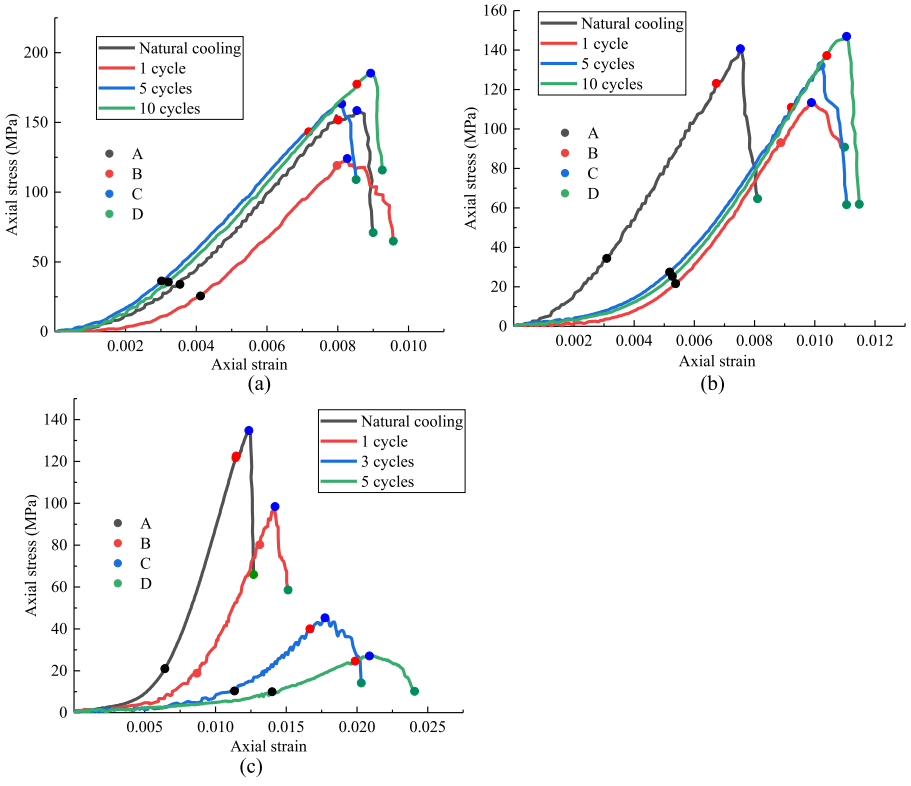

Fig. 5. Stress–strain curves at various temperatures and cycle numbers: (a) 200 °C; (b) 400 °C and (c) 600 °C.

3.2. Heating and water cooling cycles

Fig. 5 illustrates the axial stress-strain curves after different numbers of heating-water cooling cycles. Similar to the natural cooling process, these curves can be categorized into four stages. Compared to natural cooling, the peak strength significantly decreased after a single water cooling cycle. This reduction can be attributed to the higher thermal stress generated during thermal shock caused by rapid cooling in a constant-temperature water bath at 20 °C. The intensified thermal stress led to greater damage and fracturing within the sample.

Figs. 6a and 7a respectively depict the variations in peak strength with increasing temperature and number of cycles. At temperatures of 200 °C and 400 °C, the peak strength exhibits an increasing trend with an increase in the number of cycles. This phenomenon can be attributed to two factors. Firstly, the heating-water cooling process has the potential to close natural cracks present in the sample, contributing to the observed increase in strength. Secondly, as granite is a heterogeneous material, different thermal expansion coefficients among its mineral particles result in uneven thermal stress distribution at high temperatures. During the heating process, some particles expand and fill existing cracks. Although the sample experiences damage and cracking due to temperature differences during the heating-water cooling process, the cooling temperature difference is small. As a result, the weakening effect on the sample's strength is less significant compared to the strength improvement achieved through the elimination of uneven thermal stress. Consequently, the sample's strength improves upon cooling. However, when the heating temperature reaches 600 °C, the cooling temperature difference becomes more substantial, intensifying the damage and fractures within the sample. In this case, the weakening effect outweighs the strength improvement effect after cooling, leading to a significant decrease in peak strength as the number of cycles increases. The changing trends of peak strength in Figs. 6a and 7a similarly indicate the existence of a temperature threshold between 400 °C and 600 °C. When the temperature is below 600 °C, the influence of temperature and the number of cycles on the specimen's peak strength is far less significant compared to when the temperature exceeds 600 °C.

Figs. 6b and 7b illustrate the variations in peak strain under different temperature and number of cycle conditions.Irrespective of the temperature, the peak strain demonstrates an increasing trend as the number of cycles increases. This suggests that as the number of cycles increases, the sample becomes less brittle, and the peak strain becomes higher. Furthermore, the increase in peak strain is more pronounced at higher temperatures and with a greater number of cycles.

Figs. 6c and 7c, as well as Figs. 6d and 7d, respectively depict the variations of elastic modulus and deformation modulus under different temperature and number of cycle conditions. When the temperature is 200 °C and 400 °C, there is no significant correlation observed between the elastic modulus and the number of cycles. However, at a heating temperature of 600 °C, the elastic modulus decreases as the number of cycles increases. Specifically, the elastic modulus is 13.7 GPa, 4.9 GPa, and 2.6 GPa for 1, 3, and 5 cycles, respectively. It is worth noting that after 3 cycles, the elastic modulus remains relatively low (less than 5 GPa), and the degree of weakening does not increase with further increases in the number of cycles. Furthermore, as seen inFig. 6d and Fig. 7d, the deformation modulus increases with an increase in the number of cycles at 200 °C and 400 °C, but decreases as the number of cycles increases at 600 °C. Notably, the values of the deformation modulus are similar when the number of cycles is 5 and 10. This suggests that if the temperature difference between heating and cooling is not sufficiently high, the influence on the deformation characteristics becomes relatively minor when the number of cycles exceeds 5.

3.3. Failure mode

To describe the failure mode observed in this experiment, the work conducted by Tian et al. [31] was considered, who used three basic types

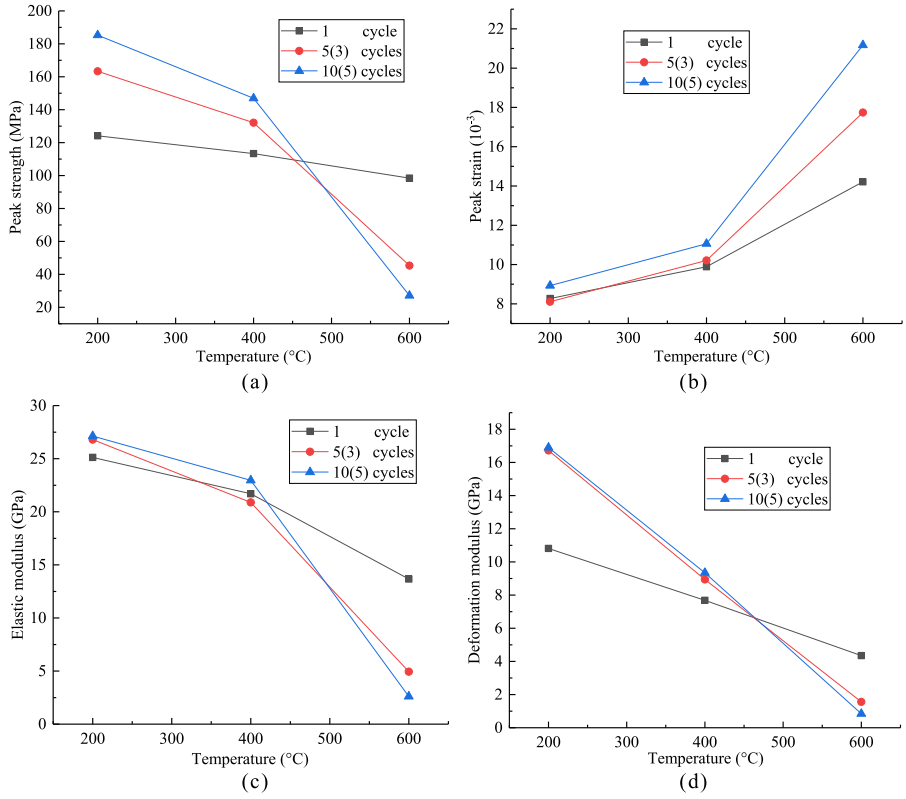

Fig. 6. Mechanical parameters after heating–water cooling process at different temperatures: (a) Peak strength; (b) Peak strain; (c) Elastic modulus and (d) Deformation modulus.

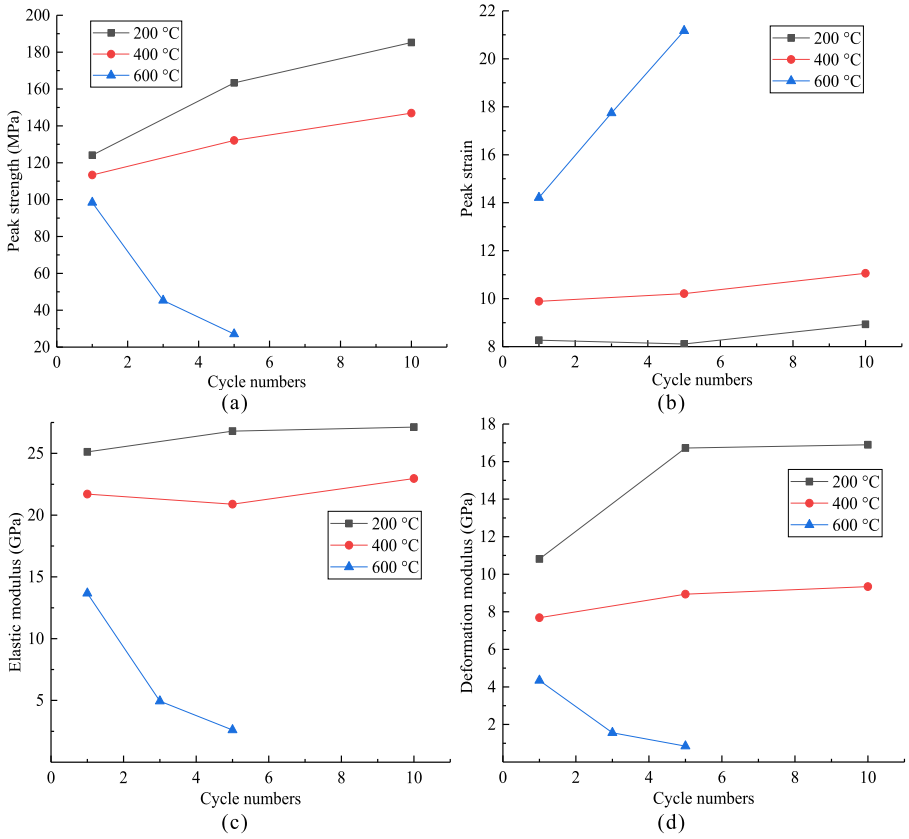

Fig. 7. Mechanical parameters after heating–water cooling process at different cycle numbers: (a) Peak strength; (b) Peak strain; (c) Elastic modulus and (d) Deformation modulus.

(Fig. 8) of rock failure mechanisms. Generally, a crack with a nearly vertical penetration results in a tensile failure mode (T-mode), a penetrating crack with a certain inclination brings about a shear failure mode (S-mode),and the mode with both tensile and shear cracks is mixed tensile–shear failure mode (TS-mode).

Fig. 9 is illustrated the failure modes observed during heating and natural cooling at different temperatures. As the temperature increases, the failure mode undergoes a transformation: from T mode at 20 °C to TS mode at 200 °C and 400 °C, and finally to S mode at 600 °C. Fig. 10 presents the failure modes under various temperatures and cycle numbers. At 200 °C, an increase in cycle numbers causes the failure mode to shift from T mode to TS mode, while still exhibiting brittle failure characteristics. The moment of failure releases a substantial amount of elastic energy, resulting in the fracturing of large rock blocks. At 400 °C, the failure modes vary depending on the cycle numbers, exhibiting both

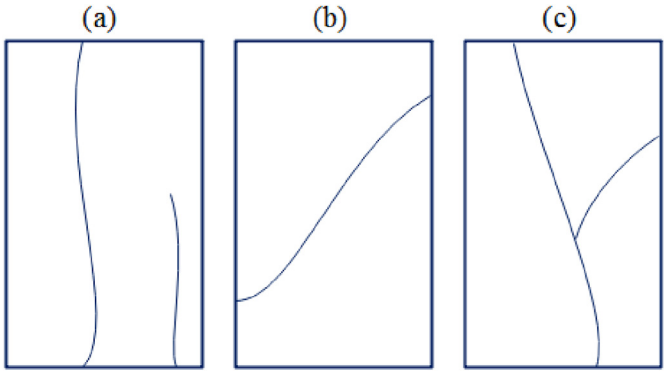

Fig. 8. Three failure modes of granite samples (modified from the study by Tian et al. [31]): (a) T-mode; (b) S-mode and (c) TS-mode.

TS and S modes. The transition from brittle to plastic failure occurs, leading to a significant reduction in the size of damaged blocks. At 600 °C, the failure mode is consistently identified as S mode. Comparatively, the plastic failure characteristics become more pronounced with fewer cycles (3 and 5 cycles). The sample undergoes a shift from flaky spalling to granular spalling, with the complete failure resulting in the generation of a substantial amount of granular rock powder.

With increasing temperature, the mineral particles in the rock undergo volume expansion, giving rise to nonuniform thermal stress. This expansion causes the particles to exert pressure on each other, similar to the application of compressive stress on the mineral interfaces and internal microfracture surfaces. Concurrently, higher heating temperatures lead to a greater initiation of microcracks within the sample and a decrease in the original cohesion and friction, resulting in reduced shear strength. Moreover, an increase in the number of heating cycles amplifies the formation of microcracks in the rock, further weakening its structural integrity. Consequently, as temperature and cycle numbers increase, shear failure gradually becomes the predominant mode of failure, with temperature playing a crucial controlling role.

3.4. Discussion on thermal damage mechanism

The effect of high temperature on granite samples can be summarized in two aspects. Firstly, elevated temperatures cause the separation and decomposition of interlayer water, crystal water, and structural water present in the rock. This results in the formation of mineral combinations with minimal or no water content, leading to changes in the rock's composition and subsequent changes in its mechanical properties. Fig. 11 illustrates granite samples after undergoing heating and natural cooling cycles at various temperatures. As the heating temperature increases, the color of the rock surface transitions from yellow to red and gradually deepens. This change in color is attributed to the original yellow iron

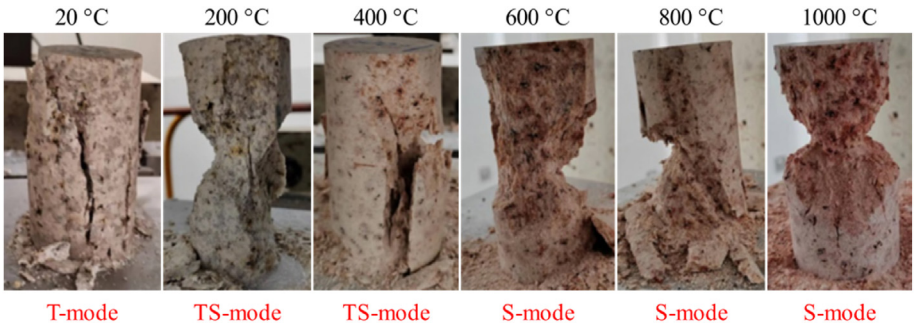

Fig. 9. Failure modes after heating–natural cooling process.

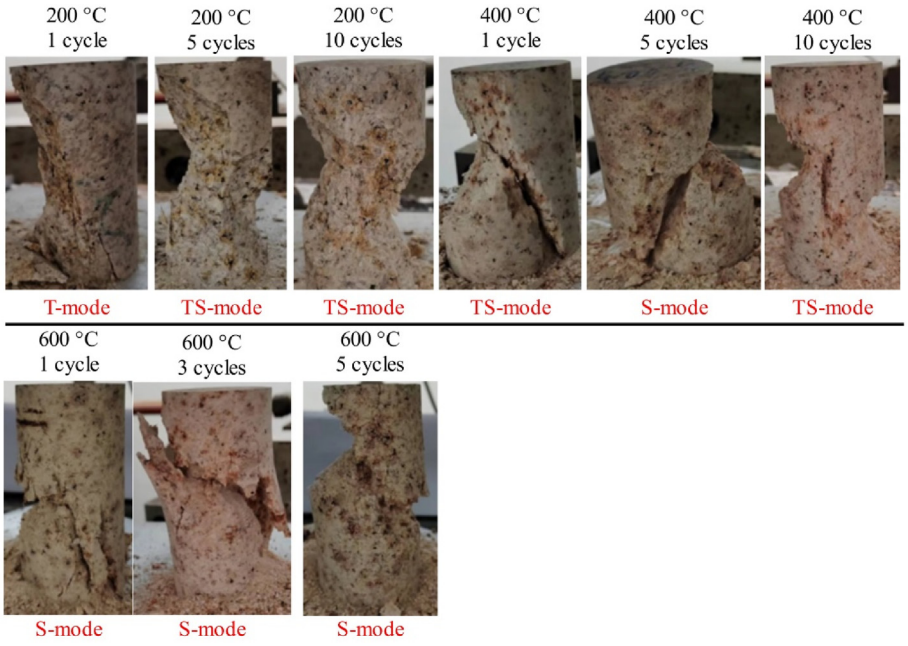

Fig. 10. Failure modes after heating–water cooling process.

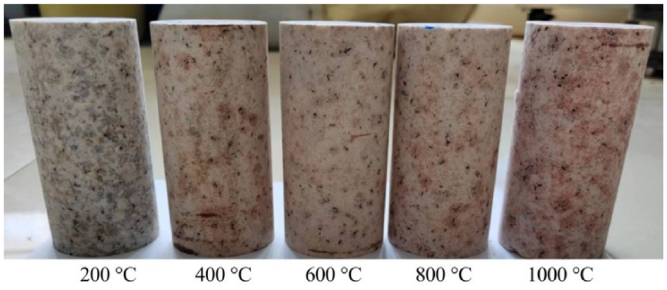

Fig. 11. Samples after heating–natural cooling cycles at different temperatures.

oxide present in the granite sample, which transforms from hydrated iron oxide ($Fe_2O_3 \cdot xH_2O$) to red iron oxide (Fe_2O_3) through dehydration and discoloration. The chemical reaction can be represented as follows:

$$Fe_2O_3 \cdot xH_2O \overset{\text{Heating}}{\rightarrow} Fe_2O_3 + xH_2O$$

On the other hand, as granite is a heterogeneous material, there are variations in the thermal expansion coefficients of its mineral particles (see Fig. 12). Consequently, when the temperature changes, the rock undergoes uncoordinated thermal deformation, generating thermal stress. This thermal stress can lead to thermal damage and thermal fractures, ultimately deteriorating the mechanical properties of the rock. Fig. 13 displays samples after undergoing a heating and water cooling process. Compared to samples heated to 200 °C and 400 °C, those heated to 600 °C exhibit a higher number of visible macroscopic cracks on the sample surface. Furthermore, as the number of heating cycles increases, the number and length of these cracks also increase. After five cycles, some cracks merge together, significantly compromising the mechanical properties of the rock. By considering Figs. 4 and 7 together, it can be concluded that temperature is the primary factor influencing the mechanical and deformation properties. Only when the heating temperature exceeds 400 °C the peak strength and elastic modulus of the rock notably decrease with an increase in the number of cycles, while plasticity becomes more pronounced. However, when the heating temperature is equal to or below 400 °C, the peak strength increases with the number of cycles, and the influence of cycle numbers on the deformation characteristics of the rock is not evident. This also indicates that compared to the number of cycles, temperature is the predominant factor driving changes in the deformation characteristics of specimen strength. Only when the heating temperature surpasses the temperature threshold, does the influence of an increasing number of cycles on the rock's strength deformation characteristics become more significant.

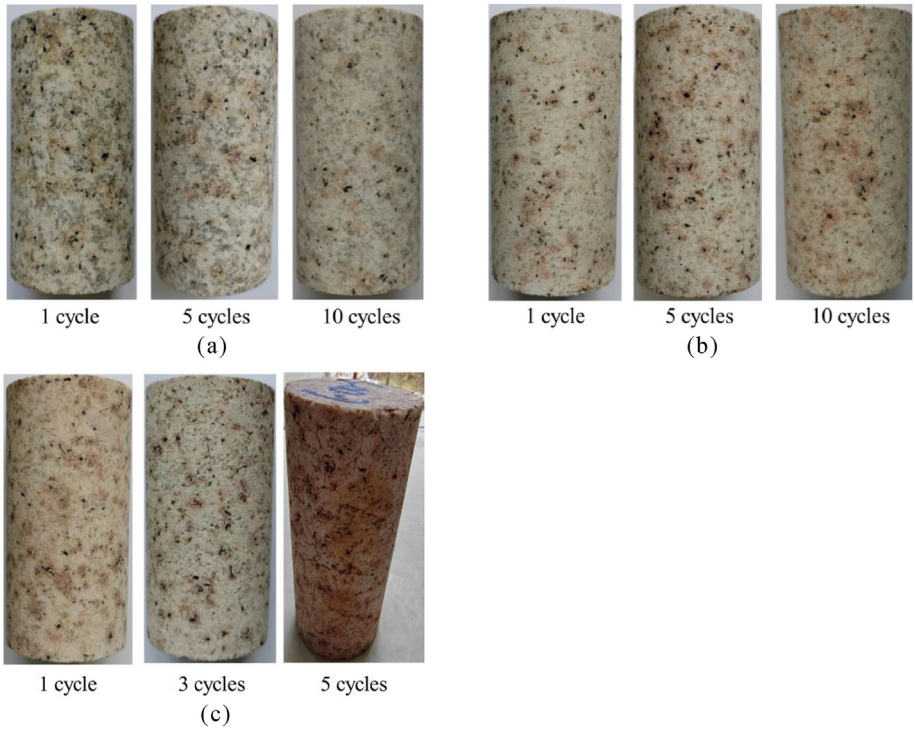

Fig. 12. Samples after heating–water cooling cycles at different temperatures:(a) 200 °C; (b) 400 °C and (c) 600 °C.

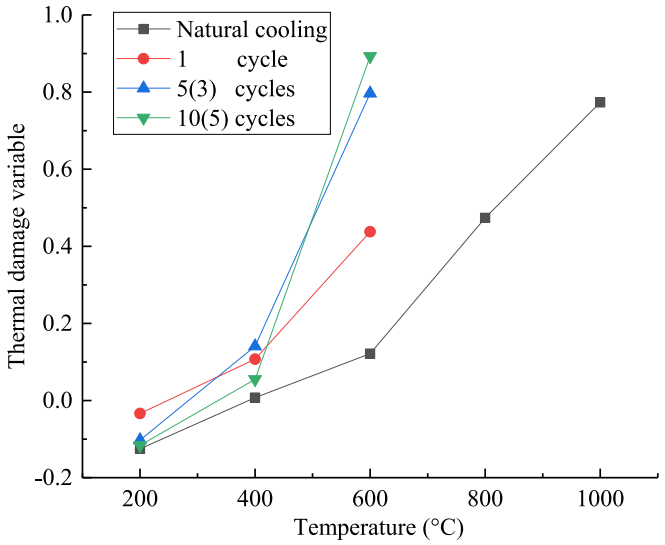

Fig. 13. Change in the thermal damage variables under different cooling modes and cycle numbers.

4. Constitutive model

4.1. Statistical damage constitutive relationship

The model assumptions are as follows: (1) Rock damage is isotropic; (2) Heat transfer in the rock is only solely through heat conduction, without considering heat convection and heat radiation; (3) Rock microelements obey Hooke's law before experiencing damage; (4) The rock consists of random and heterogeneous particles, and the strength of the microelements follows a certain statistical distribution.

Based on the above experimental results, an increase in the temperature and number of cycles will result in a large number of microcracks inside the rock, resulting in a significant reduction in the elastic modulus compared with that at room temperature.Therefore, when the sample is only subjected to heating and cooling, the thermal damage variable $D_{(T,n)}$ can be expressed as:

$$D_{(T,n)} = 1 - \frac{E_{(T,n)}}{E_0} \tag{1}$$

where $E_{(T,n)}$ is the elastic modulus for n number of cycles and a heating temperature of T; E_0 represents the elastic modulus at 20 °C. Notably, only the cumulative damage caused by heating-cooling process is considered in this paper; the softening effect of water on the rock is not considered.

The mechanical damage variable D_M is defined as:

$$D_M = 1 - \frac{E_{TM}}{E_{(T,n)}} \tag{2}$$

Here, E_{TM} is the elastic modulus under the combined effect of temperature and mechanical loading.

The total damage variable D is expressed as:

$$D = 1 - \frac{E_{TM}}{E_0} \tag{3}$$

Substituting Eqs. (1) and (2) into (3):

$$D = D_{(T,n)} + D_M - D_{(T,n)}D_M \tag{4}$$

where $D_{(T,n)}D_M$ reflects the coupling effect of temperature and mechanical loading. The D is composed of variables related to the thermal damage, damage due to the mechanical loading, and the coupling interaction between them. Therefore, the damage variable exhibits typical nonlinear characteristics.

A rock is a typical heterogeneous material, and the Weibull probability distribution is usuallyused to describe the statistical characteristics of the heterogeneity of microelements in rock [32,33]. Therefore, the commonly used Weibull distribution function is introduced to describe the distribution of the microelement rock strength F, and the probability density function $W_{(F)}$ as follows:

$$W(F)=\frac{r}{S}\left(\frac{F}{S}\right)^{r-1}\exp\left[-\left(\frac{F}{S}\right)^{r}\right] \tag{5}$$

where S and r are the scale and shape parameters, respectively. S is called the scale parameter and represents the average value of F; r is called shape parameter, which determines the basic shape of probability density function. Similar to the thermal effect on rock damage, S and r are expressed as:

$$\begin{cases} S=S_0\left(1-D_{(T,n)}\right) \\ r=r_0\left(1-D_{(T,n)}\right) \end{cases} \tag{6}$$

Under the action of external loading, failure occurs when the stress acting on the microelement in the rock material exceeds a certain threshold. In this context, D_M can be expressed as:

$$D_M=\frac{N_d}{N_t} \tag{7}$$

where N_d is the number of microelements damaged; N_t is the total number of microelements.

When the microelement strength F exceeds a certain threshold, the number of damaged microelements can be expressed as:

$$N_d(F)=\int_0^F N_t W(F)dF=N_t\cdot\left\{1-\exp\left[-\left(\frac{F}{S}\right)^{r}\right]\right\} \tag{8}$$

Substituting Eq. (8) into Eq. (7):

$$D_M=1-\exp\left[-\left(\frac{F}{S}\right)^{r}\right] \tag{9}$$

By substituting Eqs. (2) and (9) into Eq. (4), the expression for the thermo-mechanical coupled damage variable of the rock can be obtained as follows:

$$D=1-\frac{E_T}{E_0}\cdot\exp\left[-\left(\frac{F}{S}\right)^{r}\right] \tag{10}$$

4.2. Microelement strength of rock

Previous studies [33,34] have proven that the DP criterion is suitable for describing geotechnical materials, and the parameter form is simple. Therefore, the strength of the microelement F is characterized using the DP criterion in this study as:

$$F=\lambda I_1+\sqrt{J_2} \tag{11}$$

with

$$\lambda=\frac{\sqrt{3}\sin\varphi}{3\sqrt{3+\sin^2\varphi}} \tag{12}$$

$$I_1=\sigma_x{}'+\sigma_y{}'+\sigma_z{}'=\sigma_1{}'+\sigma_2{}'+\sigma_3{}' \tag{13}$$

$$J_2=\frac{1}{6}\left[(\sigma_1{}'-\sigma_2{}')^2+(\sigma_2{}'-\sigma_3{}')^2+(\sigma_3{}'-\sigma_1{}')^2\right] \tag{14}$$

where φ is the internal friction angle; λ is a constant related to the rock properties; J_2 is the second effective deviator stress invariant; I_1 is the first invariant of the effective stress tensor; σ_1', σ_2', and σ_3' are the three effective stresses.

Figs. 4 and 6 show that when the temperature exceeds 600 °C, the high temperature enhances the plasticity of the rock. After the rock microelement is damaged, it it is also capable of transferring a portion of the compressive stress and shear stress. Therefore, there is an evident yield step in the post-peak stage of the axial stress–strain curve; as such, the correction coefficient α of the damage variable is introduced to reflect the characteristics of strain softening and residual strength of the rock:

$$\sigma_i{}'=\frac{\sigma_i}{(1-\alpha D)},\ i=1,2,3 \tag{15}$$

According to the generalized Hooke's law, the stress–strain relationship is given as:

$$E_0\varepsilon_i=\left[\sigma_i{}'-\mu\left(\sigma_j{}'+\sigma_k{}'\right)\right] \tag{16}$$

Substituting Eq. (15) into Eq. (16):

$$E_0(1-\alpha D)\varepsilon_i=\left[\sigma_i-\mu\left(\sigma_j+\sigma_k\right)\right] \tag{17}$$

Substituting Eq. (10) into Eq. (17):

$$\sigma_i=E_{(T,n)}\varepsilon_i\cdot\left\{1-\alpha+\alpha\cdot\exp\left[-\left(\frac{F}{S}\right)^{r}\right]\right\}+\mu\left(\sigma_j+\sigma_k\right) \tag{18}$$

In this study, it is considered that there is a threshold point under loadingduring the process of granite failure, and the corresponding threshold stress and strain are σ_e and ε_e. When the stress of the rock is lower than σ_e, the internal cracks in the rock have not yet started to expand, and there is no damage. When the stress value exceeds σ_e, the damage can be expressed by Eq. (10). Based on the conclusion drawn by Martin et al. [35], the threshold stress is considered to be 40% of the peak strength. Based on the stress-strain curves in Figs. 4 and 6, it can be observed that the stress-strain relationship during the initial loading stage resembles a quadratic function graph. Therefore, a quadratic function is used to fit the constitutive relationship of the rock before the threshold point. The functional relationship can be set as:

$$\sigma_i=a\varepsilon_i^2+b\varepsilon_i,\ (0\le\varepsilon\le\varepsilon_e) \tag{19}$$

In a conventional rock triaxial test, $\sigma_2=\sigma_3$, and by solving Eqs. (13) and (14), I_1 and J_2 can be expressed as:

$$I_1=\frac{(\sigma_1+2\sigma_3)E_{(T,n)}\varepsilon_1}{\sigma_1-2\mu\sigma_3} \tag{20}$$

$$\sqrt{J_2}=\frac{(\sigma_1-\sigma_3)E_{(T,n)}\varepsilon_1}{\sqrt{3}(\sigma_1-2\mu\sigma_3)} \tag{21}$$

The statistical damage constitutive model can be expressed as:

$$\sigma_i=\begin{cases} a\varepsilon_i^2+b\varepsilon_i,\ (0\le\varepsilon\le\varepsilon_e) \\ E_{(T,n)}\varepsilon_i\cdot\left\{-\alpha+1+\alpha\cdot\exp\left[-\left[\frac{1}{S}\cdot\left(\frac{\sqrt{3}\sin\varphi}{3\sqrt{3+\sin^2\varphi}}\cdot\frac{(\sigma_1+2\sigma_3)E_{(T,n)}\varepsilon_1}{-2\mu\sigma_3+\sigma_1}\right.\right.\right.\right. \\ \left.\left.\left.\left.+\frac{(\sigma_1-\sigma_3)E_{(T,n)}\varepsilon_1}{\sqrt{3}(\sigma_1-2\mu\sigma_3)}\right)\right]^{r}\right]\right\}+2\mu\sigma_3,\ (\varepsilon>\varepsilon_e) \end{cases} \tag{22}$$

4.3. Determination of constitutive model parameters

In the conventional linear fitting method, the Weibull distribution parameters lack physical significance [34]. To ensure that each parameter in Eq. (22) has a clear physical meaning, the stress and strain at the damage threshold point, as well as the peak strengthand peak strain, are introduced, and the expression for each parameter was obtained using the peak point method.

4.3.1. Parameters r and S

The following boundary conditions exist at the peak point of the curve:

$$\varepsilon_1 = \varepsilon_P, \sigma_1 = \sigma_P \tag{23}$$

$$\sigma_1 = \sigma_P, \frac{\partial \sigma_1}{\partial \varepsilon_1} = 0 \tag{24}$$

Substituting Eq. (18) into boundary conditions (23) and (24), r and S can be expressed as:

$$r = \frac{(\sigma_P - 2\mu\sigma_3)}{\left[\sigma_P + (\alpha-1)E_{(T,n)}\varepsilon_P - 2\mu\sigma_3\right] \cdot \ln \frac{\alpha E_{(T,n)}\varepsilon_P}{\sigma_P + (\alpha-1)E_{(T,n)}\varepsilon_P - 2\mu\sigma_3}} \tag{25}$$

$$S = \left(\frac{A^r}{\ln \frac{\alpha E_{(T,n)}\varepsilon_P}{\sigma_P + (\alpha-1)E_{(T,n)}\varepsilon_P - 2\mu\sigma_3}} \right)^{\frac{1}{r}} \tag{26}$$

$$A = \frac{\sqrt{3}\sin\varphi}{3\sqrt{3+\sin^2\varphi}} \cdot \frac{(\sigma_P + 2\sigma_3)E_T\varepsilon_P}{\sigma_P - 2\mu\sigma_3} + \frac{(\sigma_P - \sigma_3)E_T\varepsilon_P}{\sqrt{3}(\sigma_P - 2\mu\sigma_3)} \tag{27}$$

4.3.2. Parameters a and b

The stress and strain before and after thethreshold point are continuousand can be expressed as:

$$\sigma_e = a\varepsilon_e^2 + b\varepsilon_e = \varepsilon_e E_{(T,n)} \cdot \left\{ 1 - \alpha + \alpha \cdot \exp\left[-\left(\frac{F}{S}\right)^r \right] \right\} + 2\mu\sigma_3 \tag{28}$$

$$\begin{aligned} &\frac{\partial \sigma_1}{\partial \varepsilon_1} | \varepsilon_1 = \varepsilon_e = 2a\varepsilon_e + b \\ &= E_{(T,n)} \cdot \left\{ -\alpha + 1 + \alpha \cdot \exp\left[-\left(\frac{A}{S}\right)^r \right] \right\} + \varepsilon_e \alpha E_{(T,n)} \cdot \exp\left[-\left(\frac{A}{S}\right)^r \right] \cdot \left\{ -r \cdot \left[\left(\frac{A}{S}\right)^{r-1} \right] \right\} \cdot \frac{A}{\varepsilon_e S} \end{aligned} \tag{29}$$

The parameters a and b are obtained as follows:

$$a = \frac{B - E_{(T,n)} \cdot \left\{ 1 - \alpha + \alpha \cdot \exp\left[-\left(\frac{A}{S}\right)^r \right] \right\}}{\varepsilon_P} - \frac{2\mu\sigma_3}{\varepsilon_P^2} \tag{30}$$

$$b = 2E_{(T,n)} \cdot \left\{ 1 - \alpha + \alpha \cdot \exp\left[-\left(\frac{A}{S}\right)^r \right] \right\} + \frac{4\mu\sigma_3}{\varepsilon_P} - B \tag{31}$$

$$\begin{aligned} B = E_{(T,n)} \cdot &\left\{ -\alpha + 1 + \alpha \cdot \exp\left[-\left(\frac{A}{S}\right)^r \right] \right\} + \varepsilon_e \alpha E_{(T,n)} \cdot \exp\left[-\left(\frac{A}{S}\right)^r \right] \cdot \left\{ \right. \\ &\left. -r \cdot \left[\left(\frac{A}{S}\right)^{r-1} \right] \right\} \cdot \frac{A}{\varepsilon_e S} \end{aligned} \tag{32}$$

5. Model validation and analysis

5.1. Evolution characteristics of damage variables

Fig. 13 illustrates the variations in the thermal damage variable $D_{(T,n)}$ as calculated using Eq. (1) for different cooling modes and cycle numbers. It can be observed that the thermal damage variables at 200 °C are predominantly negative, indicating minimal damage to the rock samples under this thermal loading condition. This suggests that the closure of natural cracks and the mitigation of uneven thermal stress during heating and cooling have a significant influence on improving the elastic modulus of the rock. At temperatures of 400 °C and above, the thermal damage variable increases with the temperature rise. Among the different cooling modes, natural cooling exhibits the lowest rate of increase. Conversely, in the water cooling mode, the damage progression accelerates with higher number of cycles, leading to a more pronounced reduction in rock strength. This trend in thermal damage evolution aligns with the mechanical property analysis results mentioned earlier.

Fig. 14 illustrates the evolution characteristics of the total damage variable, calculated using Eq. (10), for different cooling modes and number of cycles. The evolution can be roughly divided into three stages. In the first stage, prior to reaching the damage threshold point, the rock remains in the elastic stage. At this point, the stress level is too low to generate new microcracks, resulting in no new damage. In the second stage, after surpassing the damage threshold point, new microcracks initiate and propagate within the rock, leading to a gradual and steady increase in damage. As internal microcracks expand and penetrate, macrocracks form, accelerating the overall rock damage. The third stage refers to a rapid stress drop, where the damage threshold approaches 1, indicating significant damage accumulation.

The rate of damage variable evolution reflects the strength and deformation characteristics of the samples. At 200 °C, the limited thermal damage results in enhanced rock strength due to cooling, thus yielding a negative damage variable during the initial loading stage. At 400 °C, the water cooling mode generates greater thermal shock, leading to increased rock damage. Therefore, the natural cooling mode exhibits the minimum damage variable during the initial loading stage. At 600 °C, as the number of cycles increase, the damage initially rises and then decreases. This behavior is attributed to the higher number of cycles inducing more thermal damage. Additionally, the increased plasticity with higher number of cycles causes the stress to drop more gradually after reaching peak strength, resulting in a more gradual rate of increase in the damage variable during later stages.

5.2. Model validation

The theoretical stress–strain curve obtained from Eq. (22) is compared with the corresponding experimental data (Fig. 15). In Fig. 15, “EC” and “TC” represent the experimental and theoretical curves, respectively. To make the fitting result more accurate, the damage correction coefficient α is uniformly taken as 0.9. Table 2 presents the experimental data and model parameter calculation results. Fig. 15 shows that the results of the theoretical model are consistent with the test results. The results obtained by the theoretical method are above the experimental curve, indicating that the theoretical model is conservative.

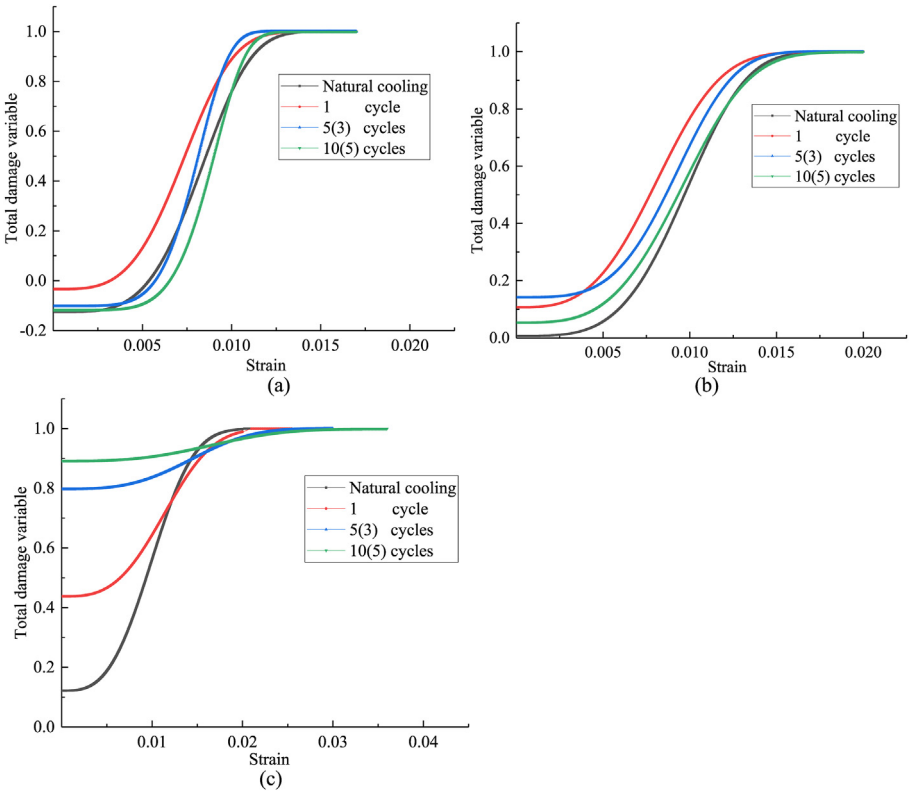

Fig. 14. Evolution characteristics of the total damage variable under different cooling modes and cycle numbers: (a) 200 °C; (b) 400 °C and (c) 600 °C.

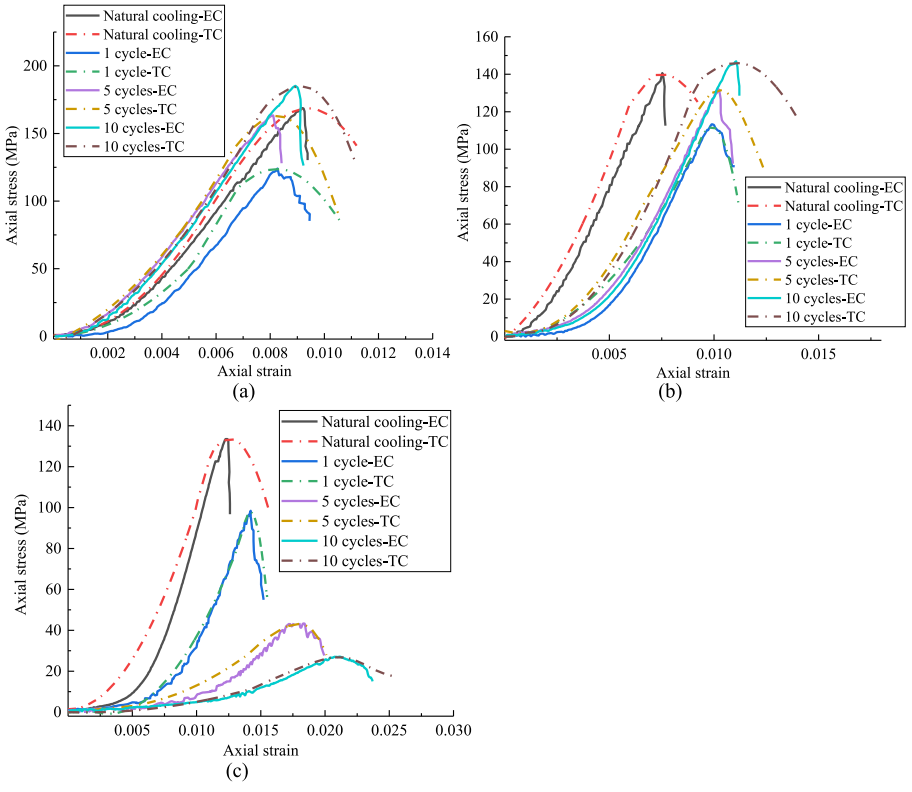

Fig. 15. Theoretical and experimental curves under different temperatures and cycles: (a) 200 °C; (b) 400 °C and (c) 600 °C.

The reasons are as follows: On the one hand, the relatively conservative DP criterion is adopted in the process of theoretical model derivation. On the other hand, when defining the thermal damage variable, it is assumed that the rock does not produce other forms of damage, which ignores the weakening of the rock strength to a certain extent. In engineering simulations, one can select parameter values in the model based on actual

Table 2
Values of constitutive model parameters under different cooling modes and different temperatures.

Cooling mode	Temperature	Cycle numbers	σ_P/MPa	$\varepsilon_P/10^{-3}$	σ_e/MPa	$\varepsilon_e/10^{-3}$	$E_{(T,n)}$/GPa	μ	r	S/MPa
Natural cooling	20	–	168.77	9.182	67.508	3.6728	24.304	0.23	3.659	202.912
	200	–	158.483	8.541	63.3932	3.4164	27.353	0.19	3.872	202.451
	400	–	140.657	7.530	56.2628	3.012	24.126	0.22	4.119	210.360
	600	–	134.749	12.361	53.8996	4.9444	21.351	0.21	3.038	190.732
	800	–	79.868	13.752	31.9472	5.5008	12.789	0.23	1.315	166.091
	1000	–	47.181	17.232	18.8724	6.8928	5.511	0.18	0.719	118.601
Water cooling	200	1	124.115	8.272	49.646	3.3088	25.119	0.24	3.679	160.840
		5	163.311	8.114	65.3244	3.2456	26.796	0.23	3.908	180.461
		10	185.251	8.931	74.1004	3.5724	27.128	0.23	3.204	211.712
	400	1	113.349	9.891	45.3396	3.9564	21.7	0.19	3.238	158.671
		5	132.122	10.210	52.8488	4.084	20.883	0.17	3.109	188.281
		10	146.932	11.061	58.7728	4.4244	22.965	0.22	2.953	194.052
	600	1	98.427	14.212	39.3708	5.6848	13.669	0.21	2.121	139.891
		3	45.297	17.743	18.1188	7.0972	4.944	0.24	1.466	63.960
		5	27.105	21.171	10.842	8.4684	2.606	0.23	0.582	39.175

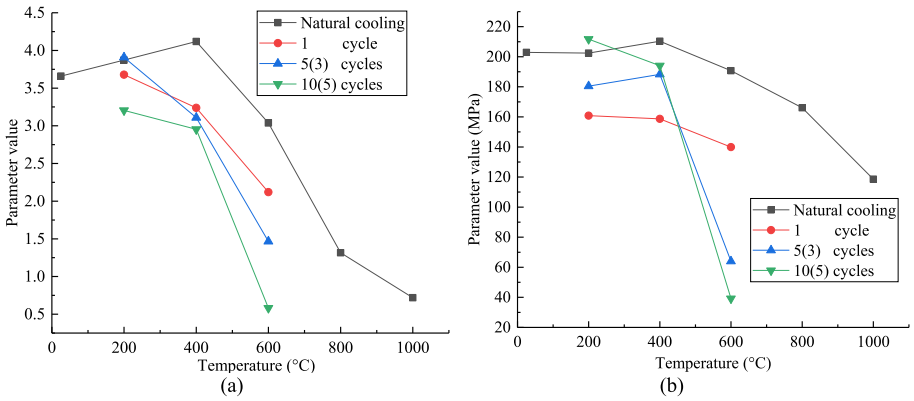

Fig. 16. Variations in parameters r and S with temperature and number of cycles: (a) r and (b) S.

environmental temperatures of the engineering site and the anticipated number of water cooling cycles. If needed, interpolation or fitting methods can be employed, potentially utilizing the data in Table 2 as a foundation. It should be noted that the model parameters in this study are derived from indoor experiments. In real-world engineering applications, differences in rock dimensions, depth, in-situ stress, and other factors might result in significant variations in parameter values. Therefore, parameter selection for engineering simulations needs to consider a comprehensive understanding of the actual environment, conditions, and the accuracy of the model.

At heating temperatures of 200 °C and 400 °C, in the post-peak stage in the post-peak stage drops sharply, while the theoretical curve shows some ductility. This is because the theoretical model considers that the sample still has a certain residual strength. On the other hand, the displacement loading method was adopted in this experiment, which has some shortcomings in the collection of post-peak data, and a subsequent triaxial test should be conducted for verification. When the temperature is 600 °C and the cycle numbers are 5 and 10, the failure mode changes from brittle failure to plastic failure. The theoretical and test results are consistent, demonstrating that the introduction of the damage correction coefficient α helped accurately reflecting the change of characteristics from brittle to ductile after heating–water cooling.

5.3. Parameter analysis

Fig. 16 illustrates the variations of parameters r and S. As the temperature increases, the parameter r generally shows a downward trend in the natural cooling mode. At 800 °C and 1000 °C, the r values are notably lower at 1.315 and 0.719, respectively, compared to other temperatures. In the water cooling mode, the r value decreases with an increase in cycle numbers. The r value can be understood as an indicator of reflects the brittleness of the samples, as supported by the curves shown in Figs. 4 and 6. A higher r value indicates greater sample brittleness.

Regarding the parameter S, it decreases as temperature increases in the natural cooling mode. In the water cooling mode, S increases at 200 °C and 400 °C with an increase in cycle numbers, but decreases at 600 °C. This indicates that S can be utilized as an indicator reflecting the macrostrength of the rock. A higher S value corresponds to a greater peak strength, aligning with the experimentally observed mechanical characteristics.

6. Conclusions

The effects of heating followed by natural cooling and heating followed by water cooling cycles on the mechanical characteristics of yellow rust granite samples were investigated through experiments. A thermo-mechanical coupled damage statistical model was developed and validated. Several key conclusions can be drawn from the study.

(1) In the natural cooling mode, heating temperatures below 400 °C had no significant influence on the rock's behavior. However, a temperature threshold was observed between 400 °C and 600 °C. Beyond this threshold, the strength properties deteriorated significantly, and the failure of the rock changed from brittle failure to ductile failure.
(2) In the water cooling mode, at temperatures below 400 °C, the peak stress increased with an increase in cycle numbers, while the elastic modulus there was no clear correlation with cycle numbers. At 600 °C, the peak stress notably decreased with an increase in cycle numbers. Regardless of temperature, the peak strain

increased, and the rock exhibited reduced brittleness with higher heating temperatures and cycle numbers.

(3) In both the natural cooling and water cooling cycle modes, as the temperature and cycle numbers increase, the failure mode gradually shifts from T-mode to S-mode, with temperature playing a controlling role in determining the failure mode.

(4) A damage constitutive model considering the thermo-mechanical coupling effect was developed for granite. And it was validated by comparing it with experimental results. In this model, the parameters *r* and S of the Weibull distribution function were found to be positively correlated with the rock's brittleness and compressive strength, respectively.

Declaration of competing interest

The authors declare that there are no known conflicts of interest associated with this manuscript.

Acknowledgements

This work was funded by the Postgraduate Research & Practice Innovation Program of Jiangsu Province (KYCX22_0613), National Natural Science Foundation of China (Grant Nos. 41831278, 51878249).

References

[1] J. Zhang, Y. Shen, G. Yang, H. Zhang, Y. Wang, X. Hou, et al., Inconsistency of changes in uniaxial compressive strength and P-wave velocity of sandstone after temperature treatments, J. Rock Mech. Geotech. Eng. 13 (2021) 143–153, https://doi.org/10.1016/j.jrmge.2020.05.008.

[2] L. Zhou, Z. Zhu, X. Xie, Y. Hu, Coupled thermal–hydraulic–mechanical model for an enhanced geothermal system and numerical analysis of its heat mining performance, Renew. Energy 181 (2022) 1440–1458, https://doi.org/10.1016/j.renene.2021.10.014.

[3] F. Zhang, J. Zhao, D. Hu, F. Skoczylas, J. Shao, Laboratory investigation on physical and mechanical properties of granite after heating and water-cooling treatment, Rock Mech. Rock Eng. 51 (2018) 677–694, https://doi.org/10.1007/s00603-017-1350-8.

[4] S.Q. Yang, Y.H. Huang, W.L. Tian, P.F. Yin, H.W. Jing, Effect of high temperature on deformation failure behavior of granite specimen containing a single fissure under uniaxial compression, Rock Mech. Rock Eng. 52 (2019) 2087–2107, https://doi.org/10.1007/s00603-018-1725-5.

[5] F. Yang, W. Feng, L. Matti, Y. Yang, I. Merkouriadi, R. Cen, et al., Simulation and seasonal characteristics of the intra-annual heat exchange process in a shallow ice-covered lake, Sustain. Times 12 (2020) 7832–7849, https://doi.org/10.3390/SU12187832.

[6] X. Wu, Z. Huang, X. Dai, H. Song, S. Zhang, Thermo-coupled FSI analysis of LN2 jet impinging on hot dry rock, Appl. Therm. Eng. 165 (2020) 114621, https://doi.org/10.1016/j.applthermaleng.2019.114621.

[7] L. Zhou, Z. Zhu, X. Xie, Performance analysis of enhanced geothermal system under thermo-hydro-mechanical coupling effect with different working fluids, J. Hydrol. 624 (2023) 129907, https://doi.org/10.1016/j.jhydrol.2023.129907.

[8] H. Xu, X. Lai, P. Shan, Y. Yang, S. Zhang, B. Yan, et al., Energy dissimilation characteristics and shock mechanism of coal-rock mass induced in steeply-inclined mining: comparison based on physical simulation and numerical calculation, Acta Geotech 18 (2023) 843–864, https://doi.org/10.1007/s11440-022-01617-2.

[9] C. Li, Y. Hu, T. Meng, C. Zhang, R. Gao, P. Jin, et al., Mode-I fracture toughness and mechanisms of Salt-Rock gypsum interlayers under real-time high-temperature conditions, Eng. Fract. Mech. 240 (2020) 107357, https://doi.org/10.1016/j.engfracmech.2020.107357.

[10] T. Yin, S. Zhang, X. Li, L. Bai, A numerical estimate method of dynamic fracture initiation toughness of rock under high temperature, Eng. Fract. Mech. 204 (2018) 87–102, https://doi.org/10.1016/j.engfracmech.2018.09.034.

[11] T. Guo, S. Tang, S. Liu, X. Liu, W. Zhang, G. Qu, Numerical simulation of hydraulic fracturing of hot dry rock under thermal stress, Eng. Fract. Mech. 240 (2020) 107350, https://doi.org/10.1016/j.engfracmech.2020.107350.

[12] G. Jiang, J. Zuo, L. Li, T. Ma, X. Wei, The evolution of cracks in maluanshan granite subjected to different temperature processing, Rock Mech. Rock Eng. 51 (2018) 1683–1695, https://doi.org/10.1007/s00603-018-1403-7.

[13] X. Wu, Z. Huang, H. Song, S. Zhang, Z. Cheng, R. Li, et al., Variations of physical and mechanical properties of heated granite after rapid cooling with liquid nitrogen, Rock Mech. Rock Eng. 52 (2019) 2123–2139, https://doi.org/10.1007/s00603-018-1727-3.

[14] S. Sha, G. Rong, Z. Chen, B. Li, Z. Zhang, Experimental evaluation of physical and mechanical properties of geothermal reservoir rock after different cooling treatments, Rock Mech. Rock Eng. 53 (2020) 4967–4991, https://doi.org/10.1007/s00603-020-02200-5.

[15] G. Rong, S. Sha, B. Li, Z. Chen, Z. Zhang, Experimental investigation on physical and mechanical properties of granite subjected to cyclic heating and liquid nitrogen cooling, Rock Mech. Rock Eng. 54 (2021) 2383–2403, https://doi.org/10.1007/s00603-021-02390-6.

[16] S. Akdag, M. Karakus, A. Taheri, G. Nguyen, H. Manchao, Effects of thermal damage on strain burst mechanism for brittle rocks under true-triaxial loading conditions, Rock Mech. Rock Eng. 51 (2018) 1657–1682, https://doi.org/10.1007/s00603-018-1415-3.

[17] Z nan Zhu, H. Tian, Jiang G. sheng, W. Cheng, Effects of high temperature on the mechanical properties of Chinese marble, Rock Mech. Rock Eng. 51 (2018) 1937–1942, https://doi.org/10.1007/s00603-018-1426-0.

[18] F. Wang, H. Konietzky, Thermo-mechanical properties of granite at elevated temperatures and numerical simulation of thermal cracking, Rock Mech. Rock Eng. 52 (2019) 3737–3755, https://doi.org/10.1007/s00603-019-01837-1.

[19] X. Wu, Z. Huang, S. Zhang, Z. Cheng, R. Li, H. Song, et al., Damage analysis of high-temperature rocks subjected to LN2 thermal shock, Rock Mech. Rock Eng. 52 (2019) 2585–2603, https://doi.org/10.1007/s00603-018-1711-y.

[20] Y. Qin, H. Tian, N.X. Xu, Y. Chen, Physical and mechanical properties of granite after high-temperature treatment, Rock Mech. Rock Eng. 53 (2020) 305–322, https://doi.org/10.1007/s00603-019-01919-0.

[21] D. Zhu, H. Jing, Q. Yin, S. Ding, J. Zhang, Mechanical characteristics of granite after heating and water-cooling cycles, Rock Mech. Rock Eng. 53 (2020) 2015, https://doi.org/10.1007/s00603-019-01991-6. –25.

[22] L. Weng, Z. Wu, Q. Liu, Influence of heating/cooling cycles on the micro/macrocracking characteristics of Rucheng granite under unconfined compression, Bull. Eng. Geol. Environ. 79 (2020) 1289–1309, https://doi.org/10.1007/s10064-019-01638-4.

[23] F. Zhao, Z. Shi, Q. Sun, Fracture mechanics behavior of jointed granite exposed to high temperatures, Rock Mech. Rock Eng. 54 (2021) 2183–2196, https://doi.org/10.1007/s00603-021-02393-3.

[24] M. Gao, T. Li, T. Wei, L. Meng, A statistical constitutive model considering deterioration for brittle rocks under a coupled thermal-mechanical condition, Geofluids 2018 (2018) 1–10, https://doi.org/10.1155/2018/3269423.

[25] J. Deng, D. Gu, On a statistical damage constitutive model for rock materials, Comput. Geosci. 37 (2011) 122–128, https://doi.org/10.1016/j.cageo.2010.05.018.

[26] W.G. Cao, H. Zhao, X. Li, Y.J. Zhang, Statistical damage model with strain softening and hardening for rocks under the influence of voids and volume changes, Can. Geotech. J. 47 (2010) 857–871, https://doi.org/10.1139/T09-148.

[27] W. Cao, C. Zhang, M. He, T. Liu, Deformation simulation of brittle rock based on micromechanical properties, Rock Soil Mech. 37 (2016) 2753–2760, https://doi.org/10.16285/j.rsm.2016.10.003.

[28] C. Zhang, Q. Yang, W. Cao, Study of damage constitutive model of brittle rock considering post-peak stress dropping rate, Rock Soil Mech. 40 (2019) 3099–3106, https://doi.org/10.16285/j.rsm.2018.0916.

[29] L. Zhou, S. Zhu, Z. Zhu, Cosserat ordinary state-based peridynamic model and numerical simulation of rock fracture, Comput. Geotech. 155 (2023) 105240, https://doi.org/10.1016/j.compgeo.2022.105240.

[30] H. Jiang, A. Jiang, F. Zhang, X. Yang, Study on mechanical properties and statistical damage constitutive model of red sandstone after heating and water-cooling cycles, Int. J. Damage Mech. 31 (2022) 975–998, https://doi.org/10.1177/10567895221087714.

[31] H. Tian, M. Ziegler, T. Kempka, Physical and mechanical behavior of claystone exposed to temperatures up to 1000°C, Int. J. Rock Mech. Min. Sci. 70 (2014) 144–153, https://doi.org/10.1016/j.ijrmms.2014.04.014.

[32] L. Zhou, S. Zhu, Z. Zhu, X. Xie, Simulations of fractures of heterogeneous orthotropic fiber-reinforced concrete with pre-existing flaws using an improved peridynamic model, Materials 15 (2022) 3977, https://doi.org/10.3390/ma15113977.

[33] Z. Chen, S. Sha, L. Xu, J. Quan, G. Rong, M. Jiang, Damage evaluation and statistic constitutive model of high-temperature granites subjected to liquid nitrogen cold shock, Rock Mech. Rock Eng. 55 (2022) 2299–2321, https://doi.org/10.1007/s00603-022-02779-x.

[34] Xu X. li, M. Karakus, F. Gao, Z zhen Zhang, Thermal damage constitutive model for rock considering damage threshold and residual strength, J Cent South Univ 25 (2018) 2523–2536, https://doi.org/10.1007/s11771-018-3933-2.

[35] C.D. Martin, N.A. Chandler, The progressive fracture of Lac du Bonnet granite, Int. J. Rock Mech. Min. Sci. 31 (1994) 643–659, https://doi.org/10.1016/0148-9062(94)90005-1.